DOI: XXX-XXX-XXXX

Force Reflecting Joystick Control for Applications to Bilateral Teleoperation in Construction Machinery

Dinh Quang Truong[1], Bui Ngoc Minh Truong[2], Nguyen Thanh Trung[2], Syed Abu Nahian[2], and Kyoung Kwan Ahn[2,#]

1 Warwick Manufacturing Group (WMG), University of Warwick, Coventry CV4 7AL, UK
2 School of Mechanical Engineering, University of Ulsan, Daehakro 93, Namgu, Ulsan, South Korea,680-749
Corresponding Author / E-mail: kkahn@ulsan.ac.kr, TEL: +82-52-259-2282 , FAX: +82-52-259-1680

KEYWORDS : Bilateral teleoperation system, force reflecting joystick control, recursive least square method, fuzzy logic, self-tuning

This paper presents a simple and effective force reflecting joystick controller for applications to bilateral teleoperation in construction machinery. First, this controller is a combination of an advanced force reflecting gain tuner and two local adaptive controllers, master and slave. Second, the force reflecting gain tuner is effectively designed using recursive least square method and fuzzy logics to estimate directly and accurately the environmental characteristics and, consequently, to produce properly a force reflection. Third, the local adaptive controllers are simply designed using fuzzy technique and optimized using a smart leaning mechanism to ensure that the slave follows well any given trajectory while the operator is able to achieve truly physical perception of interactions at the remote site. An experimental master-slave manipulator is setup and real-time control tests are carried out under various environmental conditions to evaluate the effectiveness of the proposed controller.

Manuscript received: August XX, 201X / Revised: August XX, 201X / Accepted: August XX, 201X

NOMENCLATURE

F_h = operator command
F_r = reflecting force
P_r = reflecting pressure
J = joystick transfer function
M = force reflecting mechanism transfer function
S = slave transfer function
Z_e = environment transfer function
F_e = loading force from environment
k = environment stiffness
c = environment damping coefficient
g_k = scaling factor of environment stiffness
g_c = scaling factor of environment damping coefficient
x = local controller input variable
N = number of fuzzy input membership functions
θ_i = top vertex position of i^{th} triangle of input x
K = number of fuzzy output membership functions
w_k = fuzzy inference output weight
g_u = scaling factor of fuzzy inference output
u = local controller output
y_r = master/slave desired response
y = master/slave response
e = local controller control error

1. Introduction

Teleoperation has played a crucial role in remote manipulation that provides the users capacity to perform naturally manual tasks at environments away from the normal human reach[1]. This type of technology has been applied worldwide in various practical fields, such as space, underwater applications, hazardous assignments, micro-assembly, minimally invasive surgical systems, etc. Especially, teleoperation technology has been widely employed in construction machinery nowadays. Particularly, in dangerous working environment, the operator can use vision devices and joysticks to observe and control the target machine located the working place. However, to improve the control performance as well as increase the operator's task performance and feelings, haptic and force feedbacks are necessary and should be built-in the control devices.

In common, the control schemes for teleoperation systems can be classified as either compliance control or bilateral control[2].

Fig. 1 Basic configuration of a bilateral teleoperation system

In the compliance control[3-10], the contact force sensed by the slave device is not reflected back to the operator, but is used for the compliance control of the slave device. On the contrary, in the bilateral control[11-23], the contact force is reflected back to the operator. Due to having the reflection force during operation, the operator is able to achieve physical perception of interactions at the remote site similar as directly working at this site. Consequently, it improves the accuracy and safety in the teleoperated manipulation. In addition, the force reflection can enhance the human operator's task performance, for example in terms of task completion time, total contact time[12]. Thus, the bilateral control has drawn a lot of attention. Generally, a bilateral teleoperation system as shown in Fig. 1[13] includes five main components: operator, master – physical device, control logics with communication channels, slave manipulator, and environment.

There are two common architectures of bilateral teleoperation systems: position-position and position-force architectures[14,15]. In the first approach, the master position is passed to the slave device, and the slave position is passed back to the master site. Then, the reflected force applied to the operator is derived from the position difference between the two devices. However, this approach is not desirable in cases of free motion. In contrast, the position-force approach uses directly the force measured at the remote site rather than the position error. In this architecture, the contact force, sensed by a force/torque sensor mounted on the slave device, is scaled by a force reflecting gain (FRG). This scaled force is then reflected back to the operator via a force reflecting mechanism (FRM) installed at the master device. This method then provides the operator a better perception of tasks execution at the remote site.

In the position-force architecture, the FRG greatly affects the task performance and stability of the system[16]. The larger force reflecting gain, the bigger reflected force becomes. Nonetheless, reflecting huge contact forces may cause the system unstable while reflecting so small force leads to a poor sense for the operator. Therefore, the FRG should be sufficiently adjusted to obtain the good stability and transparency. Raju[17] proposed a two-port network model of a single degree of freedom remote manipulation system, and applied it to design a force controller for transmitting the contact force information from a remote port to a local port. Kim[18] suggested a control method as a combination of the bilateral control and compliance control to enlarge the FRG. However, the above methods were designed to determine the FRG without considering dissimilar characteristics between different remote environments, subsequently reducing the range of that gain. To solve that problem, Cha and Cho[19] presented a force reflection controller in which neural network was to identify the environment characteristics and then, fuzzy logic was employed to choose the suitable FRG. Nevertheless, the neural network needed to be firstly trained through a set of learning data collected from various environments. Another solution to raise the FRG was offered by Kuchenbecker and Niemeyer[20]. Although the system was more stable when facing with lager FRG values, the effectiveness in recognizing the master movements due to the human force or the reflected force was generally unfeasible when dealing with nonlinearities of the master device and operator. To overcome that shortcoming, Polushin and Lung[21] proposed a projection-based force reflection algorithm for stable bilateral teleoperation. Although the proposed algorithm based on a high-gain input observer to eliminate the master motion induced by the reflected force without changing the human perception of the environment interactions, the authors did not consider the dynamic behaviors of the operator hand. Recently, Polushin and his colleagues[22] developed a method named as generalized projection-based force reflection algorithm to solve the remained limitations in their previous studies[23]. However, those suggested solutions were not proven in practices. Although the reported algorithms bring some remarkable results, there still remain some drawbacks such as: how to determine the FRG appropriately with environments containing unknown and uncertain characteristics; and how to construct effectively the two local controllers in order to ensure that the slave executes the tasks accurately in any condition while the master site exerts properly the feedback forces on the human hand through the FRM with high nonlinear characteristics.

To deal with the aforementioned limitations in bilateral teleoperation applications, especially paying attention to construction machines, this paper presents a simple and effective force reflecting joystick controller (FRJC) with following contributions. First, this controller is a combination of an advanced force reflecting gain tuner (FRGT) and two local adaptive controllers named as self-tuning fuzzy controllers (STFCs). Second, the FRGT is effective designed to estimate directly the environmental characteristics using recursive least square method (RLSM) –based estimator and, according to the estimated results, to generate suitably the FRG using a so-called fuzzy gain tuner (FGT). Third, the STFC is simply designed using fuzzy technique and optimized using a smart learning mechanism (SLM). This STFC is then applied to both sites of the system, slave and master, to ensure that the slave follows well any given trajectory while the operator is able to achieve truly physical perception of interactions at the remote site. A test rig consisting of a bilateral teleoperation system and an environment simulator is developed and set-up to investigate the applicability of the proposed FRJC.

The rest of this paper is organized as follows: Section 2 describes configuration of a teleoperation test rig; Section 3 gives the concept as well as the design process of the FRJC; real-time experiments and discussions are then carried out in Section 4; finally, some conclusions are drawn in Section 5.

2. Teleoperation test rig setup

In order to facilitate a comprehension of the proposed FRJC method, a proper test rig has been necessarily set-up in laboratory as shown in Fig. 2. As seen in Fig. 2a, the experimental apparatus includes mainly a master-slave teleoperation system with one degree of freedom (DOF), an environment simulator and, a compatible personal computer (PC, Core TM 2 Duo 1.8 GHz processor) to build the proposed FRJC.

The master device is a 2-DOF electrical joystick, made by Sakae Co. Ltd, integrated a force reflecting mechanism as depicted in Fig. 3. Herein, the pneumatic rotary actuators from SMC Corp. are used to design the FRM which typically uses DC electric motors.

DOI: XXX-XXX-XXXX

Subsequently, it allows the FRM to generate quickly and smoothly the reflecting force which represent the interaction between the slave and the environment simulator. In order to make a wide range of reflected forces, three pneumatic rotary actuators are properly selected and connected in series (see Fig. 3). An air compressor is used to create the pressurized air source for the rotary actuators. These actuators are driven by a 5/3-way proportional valve manufactured by Festo Corp. of which the control signal is sent from the PC through a multi-function Advantech PCI-1711 card. Furthermore, the relative working pressures of these actuators are measured by two Festo pressure sensors and fed back to the PC to perform the closed loop reflected force control. By this way, the summing reflected torque can be generated on the joystick shaft up to 3Nm while the air source is at a pressure of 7bar. This reflected torque range is sufficient for providing the operator with a proper feeling of loading conditions at the slave site. The master device is then fabricated as displayed in Fig. 3. Due to the 1-DOF teleoperation system, only one axis of the joystick is selected to generate driving commands for the slave. Moving action from the operator hand applied to the joystick on this axis is detected by a potentiometer attached at one end of the corresponding joystick shaft. Through the PCI-1711 card, this action is then sent to the system controller on the PC to convert into a command for the slave.

At the slave site, the manipulator is represented by a pneumatic cylinder from Festo Corp. connected with masses which are movable on a slider (see Fig. 2). The cylinder is driven by another 5/3-way proportional Festo valve to follow any trajectory given from the master device. The valve control signal is derived by the local slave controller on the PC through the PCI-1711 card. A linear variable differential transformer (LVDT) made by Novotechnik is fixed on the rig base to measure the displacement of the piston rod and, consequently, performs the closed loop tracking control.

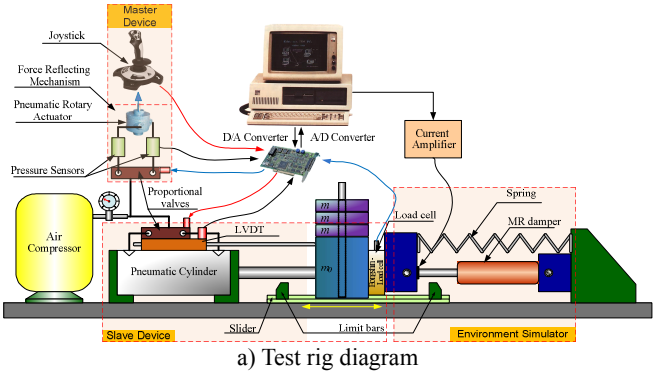

a) Test rig diagram

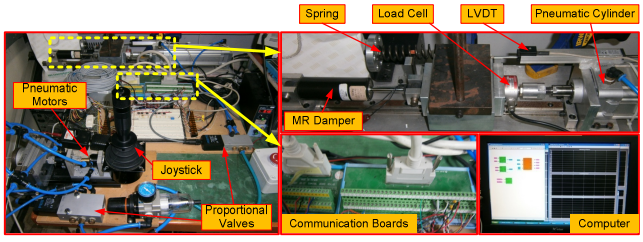

b) Photograph of test rig

Fig. 2 Experimental setup of the 1-DOF teleoperation test rig

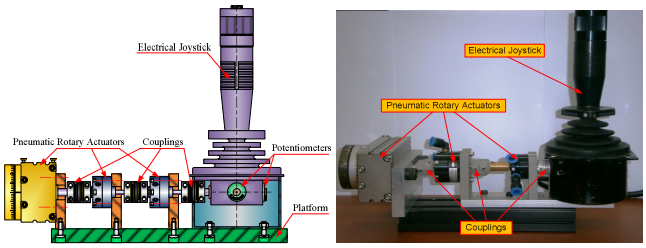

Fig. 3 Design of the master device integrated the FRM

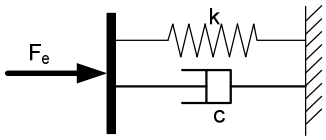

Fig. 4 Model of the environment simulator

To create various working conditions for the slave, the environment simulator is setup as a combination of a compression spring and a magneto-rheological (MR) damper from Lord Corp. in a parallel structure (as depicted in Fig. 2 and Fig. 4). This simulator is installed in the opposite direction of the pneumatic cylinder. Here, the damping force of the MR damper can be controlled by its supply current which is sent from the PC through an analog output card – Advantech PCI-1720 and a current amplifier. In addition, a compatible load cell with 500kgf capacity by Bongshin is placed between the head of piston rod and the environment simulator to sense the environment conditions.

For the system safety, two limited bars are attached as in Fig. 2a to restrict the piston movement which protects the MR damper from damages. Specifications of the system key components are listed in Table 1. The control algorithm development for the teleoperation system is then described in the next section.

Table 1 Specifications of the test rig components

Parts	Type	Component characteristics
Rotary actuators	CRB1BW15 90-D	Max. torque: 0.9 Nm
	MSQB20A	Max. torque: 1.2 Nm
Pressure sensors	SDE5-D10-Q4-V	Pressure range: 0-10 bar
Pneumatic cylinder	DSNU 20-63-PPVA	Stroke: 200 mm
		Bore diameter: 63 mm
		Rod diameter:20 mm
Servo valves	MPYE-5-1/4-010B	Control voltage range: 0-10 VDC
LVDT	Novotechnik TR100	Measurement range: 0-100 mm
Load cell	CDES-500	Capacity: 500 kgf
MR damper	RD-1005-3	Input current range: 0-2 Amp
		Stroke: 53 mm
Springs		Stiffness: 1, 8, 13, and 22 kN/m
Advantech cards	PCI 1711	2 D/A outputs, 16 A/D inputs
	PCI 1720	4 D/A outputs

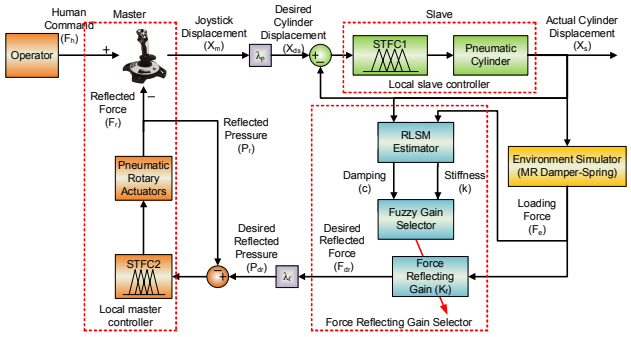

Fig. 5 Configuration of the experimental teleoperation system using the proposed FRJC

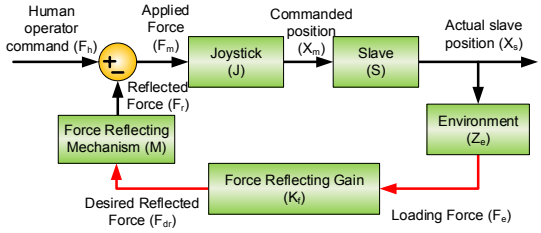

Fig. 6 Simplified control diagram of the experimental teleoperation system

3. Force reflecting joystick controller

3.1 Force reflecting joystick control concept

From Section 1, to improve performance of a bilateral teleoperation system in general as well as of the experimental system in particular, configuration of the FRJC is suggested as in Fig. 5.

The proposed algorithm is composed of three main routines: force reflecting gain tuner, local master controller, and local slave controller. During the system operation, the operator applies a moving command with force, F_h, to the joystick handle to provide a trajectory for the slave. As the joystick is moved, its displacement, X_m, is acquired and converted into a command for the slave, X_{ds}, via a suitable ratio, λ_p. The local slave controller, denoted as STFC1, attempts to make the cylinder track the given commands with high accuracy regardless any loading force due to the environment simulator, F_e. Next, the cylinder displacement (X_s) and loading force (F_e) are acquired and input to the FRGT. Here, the RLSM-based estimator firstly predicts the slave environment characteristic, represented by damping (c) and stiffness (k) factors. Next, these predicted values are fed to the FGT to produce correspondingly a value of the FRG, k_f. A reflected force, F_{dr}, is, therefore, created from the loading force using this optimal FRG. This resultant is converted approximately to a desired reflected pressure, P_{dr}, for the FRM using a transformed factor, λ_f. The local master controller, STFC2, drives the rotary actuators to generate the desired pressure and, subsequently, to generate properly the reflected force on the operator hand via the joystick handle. By this way, the operator can attain the truthful perception of the loading condition at the slave manipulator.

3.2 Stability analysis of the bilateral teleoperation system

Before designing the system control algorithm, the stability of the force reflecting teloperation system is firstly considered[15]. The FRJC-based control system presented in Fig. 5 can be simplified as shown in Fig. 6. From this figure, the slave manipulator is controlled by the operator through the joystick while the loading force sensed by the load cell is scaled and reflected back to the operator through the FRM. This forms a closed loop system and produces a stability issue. Generally, the joystick, FRM, slave manipulator, and environment can be considered as nonlinear systems, which are symbolized by $J(\bullet)$, $M(\bullet)$, $S(\bullet)$, and $Z_e(\bullet)$ transfer functions, respectively. Hence, the open loop transfer function of whole system can be expressed as

$$G(s) = k_f.Z_e(s).M(s).J(s).S(s) \tag{1}$$

In order to have a stable teleoperation system including the FRG, the sufficient condition is that the open loop DC gain, $G(0)$, should be not greater than unity:

$$G(0) = k_f.Z_{e0}.M_0.J_0.S_0 \le 1 \tag{2}$$

where J_0, M_0, S_0, and Z_{e0} in turn denote the DC gains of the J, M, S, and Z_e transfer functions. Thus,

$$k_f \le \frac{1}{Z_{e0}.M_0.J_0.S_0} \tag{3}$$

Additionally, if the slave controller is designed to drive the slave manipulator to follow accurately the given target and the master controller exerts correctly the reflected force on the human hand as desired, it is reasonable to assume that the DC gains of the S and M transfer functions are approximate unity, $S_0 \approx 1$ and $M_0 \approx 1$. Besides, the joystick is a commercial input device used in many industrial applications. Its dynamics can be represented by a transfer function of the first order lag system with constant parameters[24]. Therefore, it is able to suppose that the dynamic characteristic of the joystick remains unchanged.

From above analysis and (3), it is clear that the FRG gain should be chosen under the consideration of the environment characteristics. A small gain induces a light reflected force and, consequently, causes the operator to feel hardly the loading force so that the task performance becomes poor. Conversely, a large gain results in a strong reflected force and, thus, ensures a good task performance. However, this makes the system unstable. In summary, it can be concluded that effective designs of the FRGT, STFC1 and STFC2, are indispensable parts of a teleoperation system to achieve the good task performance and stability.

3.3 Force reflecting gain tuner – FRGT

3.3.1 Environmental characteristic estimator

In order to select the suitable FRG values, recognition of the environment dynamics is necessary and mainly based on two characteristics: stiffness and damping[25]. However, it is difficult to determine these characteristics in an online manner. And least square method (LSM) is known as one of the feasible solutions. By applying to this case, the LMS receives the position and force information of the slave device, X_s and F_e, as inputs, and bases on a model of the environment to produce two outputs, k and c, which are in turn the environmental stiffness and damping values. The environment model can be defined:

$$F_e = k.X_s + c.\dot{X}_s + F_0 \tag{4}$$

where: F_0 is included to account for a nonzero amount of the loading

DOI: XXX-XXX-XXXX

force at the initial position of the slave; $\dot{X}_s$ is the velocity of the slave derived from its position X_s.

By replacing P data sets of the slave positions and loading forces recorded at P sampling intervals into (4), a matrix relation is obtained:

$$AX = B \tag{5}$$

where: X is an unknown column vector including the parameters, k, c, and F_0 ; B is the loading force vector; A is a Px3 matrix of which each row is described as $\begin{bmatrix} X_s^p & \dot{X}_s^p & 1 \end{bmatrix}$ (the superscript p denotes p^{th} sample of the slave position and velocity).

The number of data sets (P) should be chosen sufficiently greater than three to avoid (5) becoming singularity. However, it causes the over determined problem and, generally, there is no exact solution of (5). Instead, the LSM estimates the solution of (5), X^*, by minimizing the squared error $\|AX - B\|^2$. The most well-known formula for X^* uses the pseudo-inverse of X:

$$X^* = (A^T A)^{-1} A^T B \tag{6}$$

where A^T is the transpose of A, and $(A^T A)^{-1} A^T$ is the pseudo-inverse of A.

Although (6) is concise in notation, it is expensive to compute when dealing with the matrix inversion, and may become ill-defined if $A^T A$ is singular. Moreover, much memory of the control system is cost to store the P data observations. To overcome this limitation, the modification of LSM called recursive least squared method is employed. The estimated solution, X^*, is then obtained by using sequential formulas, which allow that the computations at the present interval are implemented based on the results of the previous interval. By this way, the RLSM-based estimator requires less computational time and smaller data storage and, therefore, is suitable for online applications. Let define i^{th} row vector of matrix A in (5) as a_i and i^{th} element of vector B as b_i, X can be calculated iteratively[26] as follows:

$$\begin{aligned} X_{i+1} &= X_i + T_{i+1} a_{i+1}^T (b_{i+1} - a_{i+1} X_i) \\ T_{i+1} &= T_i - \frac{T_i a_{i+1}^T a_{i+1} T_i}{1 + a_{i+1} T_i a_{i+1}^T}, \quad i = 0,1,...,P-1 \end{aligned} \tag{7}$$

where: T_i is called the covariance matrix.

The initial conditions to launch (7) are $X_0 = 0$ and $T_0 = \gamma I$, where γ is a positive large number and I is the identity matrix of dimension 3×3. Finally, the RLSM-based estimator output, X^*, is equal to X_P. As a result, the stiffness and damping values, k and c, are determined.

3.3.2 Fuzzy gain tuner – FGT

Even if the environment characteristics are known, it is still difficult to determine properly the approximate FRG which is normally based on experience or prior knowledge about teleoperation systems. In decision making, many research works have shown that fuzzy logic which can take place of a skilled human operator is a feasible tool[19,24-27].

Thus, in this research, the fuzzy gain tuner is effectively designed and employed to specify the FRG. This FGT acquires the two outputs of the RLSM-based estimator as its inputs to create the proper FRG as an output. The FGT is composed of four parts as a general fuzzy inference illustrated in Fig. 7: fuzzy encoder, rule base, fuzzy inference engine, and fuzzy decoder.

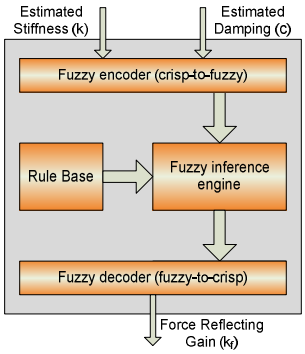

Fig. 7 Block diagram of the FGT

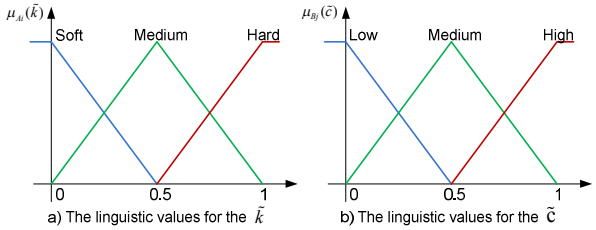

Fig. 8 The FGT – MFs of the input variables, $\tilde{k}_f, \tilde{c}$

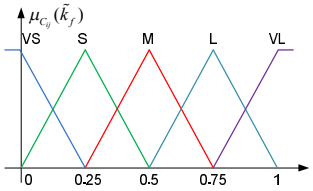

Fig. 9 The FGT – MFs of the output variables, $\tilde{k}_f$

Fuzzy encoder: The fuzzy input variables are firstly derived by normalizing the outputs of the RLSM-based estimator as follows:

$$\begin{aligned} \tilde{k} &= g_k \times k, \tilde{k} \in [0,1] \\ \tilde{c} &= g_c \times c, \ \tilde{c} \in [0,1] \end{aligned} \tag{8}$$

where: g_k and g_c denote the scaling factors for k and c, respectively. The fuzzy encoder then inspects the incoming system states, and transforms them into linguistic variables. Here, the linguistic variables of the stiffness value are described in terms of 'Soft', 'Medium', and 'Hard', while those of the damping factor are 'Low', 'Medium', and 'High' as described in Fig. 8. Triangle membership functions (MFs) are used implemented through the fuzzification.

Rule base: The rule base is utilized to interpret expert knowledge in a useful way. It contains a set of conditional sentences in the form:

$$Rule\, R_{ij} : if\ \tilde{k}\ is\ A_i\ and\ \tilde{c}\ is\ B_j\ then\ \tilde{k}_f\ is\ C_{ij} (i, j = 1,2,3) \tag{9}$$

where: $\tilde{k}_f$ is the fuzzy output variables: A_i , B_j , and C_{ij} are fuzzy subsets of the variables $\tilde{k}$, $\tilde{c}$, and $\tilde{k}_f$, correspondingly.

Table 2 Rule table for the FGT

FRG ($\tilde{k}_f$)		Stiffness		
		Soft	Medium	Hard
Damping	Low	VL	L	M
	Medium	L	M	S
	High	M	S	VS

The fuzzy output – FRG is represented by five triangle MFs named as: VS', 'S', 'M', 'L' and 'VL' which mean 'Very Small', 'Small', 'Medium', 'Large' and 'Very Large', respectively, as described in Fig. 9. Subsequently, the rule table for this FGT is established in Table 2.

Fuzzy inference engine: the inference is performed using the MAX-MIN operator. Let $\mu_{Rij}(\tilde{k}_f)$ be MF of a subset of the output which is the result of rule R_{ij}. Then, it can be obtained by:

$$\mu_{Rij}(\tilde{k}_f) = \min(\mu_{Ai}(\tilde{k}), \mu_{Bj}(\tilde{e}), \mu_{Cij}(\tilde{k}_f)) \tag{10}$$

Successively, the results of the nine rules are compared together to infer the final output MF $\mu_R(\tilde{k}_f)$ using the MAX operator:

$$\mu_R(\tilde{k}_f) = \max(\mu_{R_{11}}(\tilde{k}_f), \mu_{R_{12}}(\tilde{k}_f), ..., \mu_{R_{33}}(\tilde{k}_f)) \tag{11}$$

Fuzzy decoder: the fuzzy decoder is finally used to produce the FRG gain for the proposed FRJC, k_f as

$$k_f = g_{\tilde{k}_f} \times Defuzzify(\mu_R(\tilde{k}_f)) + k_{f0} \tag{12}$$

where: $g_{\tilde{k}_f}$ is the scaling factor for the fuzzy output variable $\tilde{k}_f$; *Defuzzify* (●) is the defuzzifier function which performs defuzzification by using the center of gravity method, and the factor; k_{f0}, is a nonzero value of the smallest force reflecting gain.

3.4 Local adaptive controllers – STFC1/STFC2

In this section, to ensure that the slave manipulates correctly any command regardless loading conditions and the FRM generates properly reflected forces as the desired values, two local controllers are implemented using fuzzy logic. However, design of a conventional fuzzy logic controller (FLC) relies largely on the user expertise in defining the MFs and fuzzy rules. The conventional FLC lacks of learning ability and adaptability and, therefore, fails to enhance the desired performance, especially when dealing with system containing high nonlinearities and large uncertainties in a noised environment. To overcome this drawback, each local controller is designed as the self-tuning fuzzy controller, which combines the fuzzy technique and the smart leaning mechanism based on Levenberg-Marquardt algorithm (LMA) as in Fig. 10.

3.4.1 Fuzzy controller design

Fuzzy inferences of each STFC is firstly considered. Each SFTC is then designed with two inputs, control error and its derivative, and one output. In case of the STFC1, the error is the difference between the desired position and the actual displacement of the cylinder while the output is the driving command for the pneumatic cylinder. Meanwhile with the STFC2, the error is the deviation of the desired reflected pressure and its actual value while the output is the driving command for the FRM.

The fuzzy input values are normalized into a range of [-1, 1], tagged as $\tilde{e}(t)$ and $d\tilde{e}(t)$, using proper scaling factors, g_e and g_{de},:

$$\begin{aligned} \tilde{e}(t) &= g_e \times e(t) \\ d\tilde{e}(t) &= g_{de} \times de(t) \end{aligned} \tag{13}$$

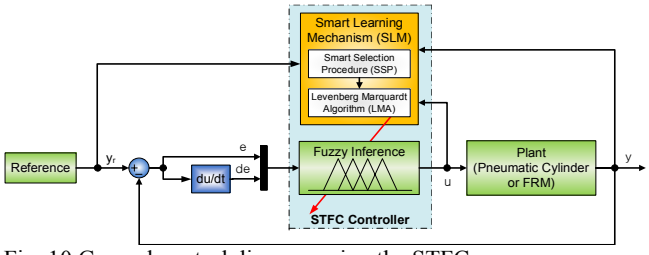

Fig. 10 General control diagram using the STFC

For each fuzzy input variable, triangle MFs are exploited as shown in Fig. 11 and can be expressed as:

$$\mu_{i,j}(x) = \begin{cases} \dfrac{x-\theta_{i-1}^j}{\theta_i^j-\theta_{i-1}^j} \; if \;\; \theta_{i-1}^j < x \le \theta_i^j \\ \dfrac{x-\theta_{i+1}^j}{\theta_i^j-\theta_{i+1}^j} \; if \;\; \theta_i^j < x \le \theta_{i+1}^j ; i = \overline{1,N} \; and \; j = 1,2 \\ 0 \quad otherwise \end{cases} \tag{14}$$

where: x is the input $\tilde{e}(t)$ or $d\tilde{e}(t)$; N is the MF number; θ_i defines the top vertex position of i^{th} triangle; j is marked to each parameter in (14) to indicate this parameter is belong to the j^{th} input $\left(x_1 \equiv \tilde{e}(t); x_2 \equiv d\tilde{e}(t)\right)$.

The fuzzy output is represented by singleton functions as illustrated in Fig. 12. Here, the weight w_k specifies the position of k^{th} singleton, and K is the number of output MFs. Based on the fuzzy sets of the input and output variables, the fuzzy rules are composed:

$$Rule\, R_{mn} : if \; \tilde{e} \, is \, A_m \wedge d\tilde{e} \, is \, B_n \Rightarrow \tilde{u} \; is \, C_k (m,n = \overline{1,N}, k = \overline{1,K}) \tag{15}$$

where: A_m, B_n and C_k are fuzzy sets of the inputs and output.

Here, the fuzzy reasoning results of the output are gained by aggregation operation of the input fuzzy sets and designed fuzzy rules, where the sum-prod aggregation method and weight average defuzzification method are used. Therefore, the fuzzy implication result for each rule of the local controller can be computed with a pair of the inputs as

$$mf(m,n) = \mu_{m,1}(\tilde{e}(t)).\mu_{n,2}(d\tilde{e}(t)) \tag{16}$$

Subsequently, the control output is derived from the fuzzy output, $\tilde{u}$ as

$$u = g_u.\tilde{u} + u_0 = g_u.\frac{\sum_{m,n=1}^{N}\left[mf(m,n).\sum_{k=1}^{K} w_k.\delta(m,n,k)\right]}{\sum_{m,n=1}^{N} mf(m,n)} + u_o \tag{17}$$

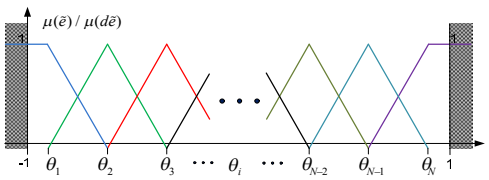

Fig. 11 The STFC - MFs of the input variables

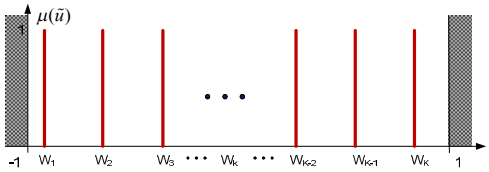

Fig. 12 The STFC - MFs of the output variable

DOI: XXX-XXX-XXXX

where g_u and u_0 are in turn the output scaling factor and offset term of the FLC output variable; $\delta(m,n,k)$ is an active factor, which is active when the output fuzzy subset in the consequent part of the rule R_{mn} is the weight w_k.

3.4.2 Smart learning mechanism

The structures of the local STFCs are online optimized using the SLM. This SLM is constructed from a so-called smart selection procedure (SSP) and Levenberg-Marquardt algorithm.

Levenberg-Marquardt algorithm: This is a standard technique used to solve non-linear least squares problems. The LMA actually acts as the gradient-descent method when the trained parameters are far from their optimal values, and as the Gauss-Newton method when the parameters are close to their optimal values.

Assuming that performance function $F(\varphi)$ required to be minimized is a sum of squares function:

$$F(\varphi)=\sum_{h=1}^{H} v_h^2(\varphi) \tag{18}$$

where: $\varphi=[\varphi_1\varphi_2...\varphi_m]^T$ is the parameter vector; $\{v_k\}$ are nonlinear functions of vector φ; H is the number of nonlinear functions. Then, the LMA minimizes the performance function $F(\varphi)$ by updating the parameter vector as

$$\varphi^{k+1}=\varphi^k+\Delta\varphi^k=\varphi^k-[J^T(\varphi^k)J(\varphi^k)+\mu I]^{-1}J^T(\varphi^k)v(\varphi^k) \tag{19}$$

where: φ^k is the parameter vector at step of time k^{th}; μ is a decisive parameter; I is the identity matrix; $v=[v_1 v_2 ... v_H]^T$ is the error vector; and $J(\varphi)$ is Jacobian matrix, which is expressed by:

$$J(\varphi)=\begin{vmatrix} \frac{\partial v_1(\varphi)}{\partial\varphi_1} & \frac{\partial v_1(\varphi)}{\partial\varphi_2} & \cdots & \frac{\partial v_1(\varphi)}{\partial\varphi_m} \\ \frac{\partial v_2(\varphi)}{\partial\varphi_1} & \frac{\partial v_2(\varphi)}{\partial\varphi_2} & \cdots & \frac{\partial v_2(\varphi)}{\partial\varphi_m} \\ \vdots & \vdots & & \vdots \\ \frac{\partial v_H(\varphi)}{\partial\varphi_1} & \frac{\partial v_H(\varphi)}{\partial\varphi_2} & \cdots & \frac{\partial v_H(\varphi)}{\partial\varphi_m} \end{vmatrix} \tag{20}$$

Self tuning fuzzy controller using LMA: Next, the LMA is applied to the designed STFCs to optimize online the MFs parameters of the fuzzy inputs $\{\theta_1^j,\theta_2^j,...,\theta_i^j,...,\theta_N^j\}$ and the weights of the output $\{w_1,w_2,...,w_k,...,w_K\}$ to minimize the control error. The performance function is defined as

$$E=\left(y(t)-y_r(t)\right)^2 \tag{21}$$

where: $y_r(t)$ and $y(t)$ are the reference input of the system and the system output at the present, respectively. Equation (21) is equivalent to the performance function in (20), where the function v and the parameters vector φ are expressed as:

$$\begin{aligned} v&=e=y(t)-y_r(t) \\ \varphi^T&=[\theta_1^1,\theta_2^1,...,\theta_N^1,\theta_1^2,\theta_2^2,...,\theta_N^2,w_1,w_2...,w_K] \end{aligned} \tag{22}$$

Therefore, the parameters of the STFC inferences can be optimized by using (19). By substituting (22) into (20), the matrix $J(\varphi)$ can be obtained as

$$J(\varphi)=\left[\frac{\partial e}{\partial\theta_1^1},...,\frac{\partial e}{\partial\theta_N^1},\frac{\partial e}{\partial\theta_1^2},...,\frac{\partial e}{\partial\theta_N^2},\frac{\partial e}{\partial w_1},...,\frac{\partial e}{\partial w_K}\right] \tag{23}$$

here, the partial derivative of the system error with respect to each fuzzy parameter is computed as the followings:

$$\frac{\partial e}{\partial w_k}=\frac{\partial e}{\partial u}.\frac{\partial u}{\partial w_k} \tag{24}$$

where:

$$\frac{\partial e}{\partial u}=\frac{\partial(y(t)-y_r(t))}{\partial u}=\frac{\partial y(t)}{\partial u}=\frac{\Delta y}{\Delta u}=\frac{y(t)-y(t-1)}{u(t)-u(t-1)} \tag{25}$$

$$\frac{\partial u}{\partial w_k}=g_u\sum_{m,n=1}^{N} mf(m,n).\delta(m,n,k) \tag{26}$$

$$\frac{\partial e}{\partial\theta_i^j}=\frac{\partial e}{\partial u}.\sum_{a=1}^{N}\frac{\partial u}{\partial\mu_{a,j}(x)}.\frac{\partial\mu_{a,j}(x)}{\partial\theta_i^j};\ i=\overline{1,N}\ and\ j=\overline{1,2} \tag{27}$$

where:

$$\frac{\partial\mu_{a,j}(x)}{\partial\theta_i^j}=\begin{cases} -\dfrac{x-\theta_{a-1}^j}{\left(\theta_a^j-\theta_{a-1}^j\right)^2} & if\ \theta_{a-1}^j<x\le\theta_a^j\ and\ \text{a=i} \\ -\dfrac{x-\theta_{a+1}^j}{\left(\theta_a^j-\theta_{a+1}^j\right)^2} & if\ \theta_a^j<x\le\theta_{a+1}^j\ and\ \text{a=i} \\ \dfrac{x-\theta_a^j}{\left(\theta_a^j-\theta_{a-1}^j\right)^2} & if\ \theta_{a-1}^j<x\le\theta_a^j\ and\ \text{a=i+1} \\ \dfrac{x-\theta_a^j}{\left(\theta_a^j-\theta_{a+1}^j\right)^2} & if\ \theta_a^j<x\le\theta_{a+1}^j\ and\ \text{a=i-1} \\ 0 & otherwise \end{cases} \tag{28}$$

$$\frac{\partial u}{\partial\mu_{a,j}(x)}=\sum_{n=1}^{N}\frac{\partial u}{\partial mf(n,a)}.\frac{\partial mf(n,a)}{\partial\mu_{a,j}(x)} \tag{29}$$

$$\frac{\partial u}{\partial mf(n,a)}=g_u.\sum_{k=1}^{K} w_k\delta(n,a,k) \tag{30}$$

$$\frac{\partial mf(n,a)}{\partial\mu_{a,j}(x)}=\mu_{a,3-j}(x) \tag{31}$$

Smart selection procedure: By using the LMA to optimize a fuzzy inference, the more MFs and rules are, the larger the number of tuning factors is. Consequently, it causes the calculation time to train the controller structure to increase considerably. In order to solve this problem, the SLM is designed as the combination of the smart selection procedure and the LMA. This SSP is implemented before the LMA learning mechanism to reduce the number of calculations when training the controllers.

From Section 3.4.1, the fuzzy inputs of each STFC are partitioned by triangle MFs in which the locations of bottom vertexes of each triangle coincide with the top vertex positions of its neighbor triangles. As a result, for a couple values of the input (x_1, x_2), there always exit input MFs which contain these values and, then, are called active input MFs (AIMFs). The output MFs corresponding to the AIMFs determined by the fuzzy rules are called active output

MFs (AOMFs). The output value of the STFC is only affected by the AIMFs and AOMFs. Therefore, the SSP is designed in such a way that, for each step using this procedure, only the AIMFs and AOMFs are detected and sent to the LMA for the optimization.

It is also realized that an arbitrary value of a fuzzy input always drops into at least one partition or maximum two partitions of this input. Hence, a couple values of the inputs (x_1, x_2) activates correspondingly at least one output MF or maximum four output MFs. The numbers of AIMFs and AOMFs can be listed into four cases in Table 3. Moreover, each the AIMF has one parameter, θ_i^j and each the AOMF has one parameter, w_k, which need to be optimized. Therefore, by using the SSP, size of the parameter vector of each STFC defined in (22), [1 x (2*N*+*K*)], can be always minimized into a range from [1 x 3] to [1 x 8] and contains only decisive parameters of AIMFs and AOMFs. As the result, this SLA saves a great deal of calculation and control process time while improves the control accuracy.

Table 3 Relation between AIMFs and AOMFs in each STFC

Number of AOMFs		Input x_2 – Number of AIMFs	
		1	2
Input x_1 – Number of AIMFs	1	1	2
	2	2	4

4 Experimental results and discussions

In this section, real-time experiments with the test rig have been done to validate the effectiveness of the proposed force reflecting joystick control approach. Firstly, the ability of the local master and slave controllers were separately investigated with pressure and position tracking control tasks, respectively. For each of these control tasks, a comparative study of using different controllers including the designed STFC (STFC1 or STFC2), a conventional proportional-integral-derivative (PID) and a fixed fuzzy logic controller (FLC) was carried out. Herein, the fuzzy inference of the STFC was built based on experience in which seven MFs were selected to present each the fuzzy input/output variable. These MFs were initially distributed as displayed in Fig. 13 while the fuzzy rules were established in Table 4. The FLC was designed as same as the STFC except the SLM. Meanwhile, the control gains of the PID were determined for each working condition using following steps:

- Step 1: the controlled system could be approximated by a transfer function. This function was derived from sets of the system input-output data using the system identification toolbox of Matlab[28];
- Step 2: the control gains were tuned for the derived transfer function using the PID tuner of Matlab/Simulink;
- Step 3: the control tests using the PID controller obtained from Step 2 were performed to refine its control gains using the trial-and-error method.

Secondly, the whole FRJC was examined for teleoperating the master-slave system under various conditions. All the control algorithms with a sampling time of 0.001*s* were built in the Simulink environment combined with the Real-time Windows Target Toolbox of Matlab.

4.1 Position tracking control

Step and chirp and sinusoidal tracking profiles were used to validate the cylinder position control using the compared controllers. Due to the application targets are construction machines[29], the chirp and sinusoidal trajectories with amplitude 15mm and a frequency range from 0.1 to 10Hz were selected. For the fuzzy designs, the input and output scaling factors, g_e, g_{de} and g_u, were assigned as 0.5, 0.02, and 1.2, respectively, while the control output offset, u_0, was set as 5.

First, the real-time experiments using the different controllers were carried out with the step and chirp profiles in the free-load condition. In this case, the PID control gains were tuned using the three steps (as described before) and consequently, derived as $k_p = 0.2, k_i = 0.15, k_d = 0.01$. The tracking results were obtained as plotted in figures 14 and 15. The results show that the control performances were quite similar when dealing with the step and low frequency tracking tasks.

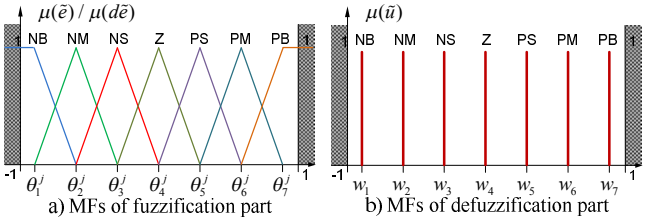

a) MFs of fuzzification part b) MFs of defuzzification part

Fig. 13. Initial MF distributions of the STFC1/STFC2 inputs/output

Table 4 Rules table of STFC1/STFC2

STFC output ($\tilde{u}$)		$\tilde{e}(t)$						
		NB	NM	NS	Z	PS	PM	PB
$d\tilde{e}(t)$	NB	NB	NB	NB	NB	NM	NS	Z
	NM	NB	NB	NB	NM	NS	Z	PS
	NS	NB	NB	NM	NS	Z	PS	PM
	Z	NB	NM	NS	Z	PS	PM	PB
	PS	NM	NS	Z	PS	PM	PB	PB
	PM	NS	Z	PS	PM	PB	PB	PB
	PB	Z	PS	PM	PB	PB	PB	PB

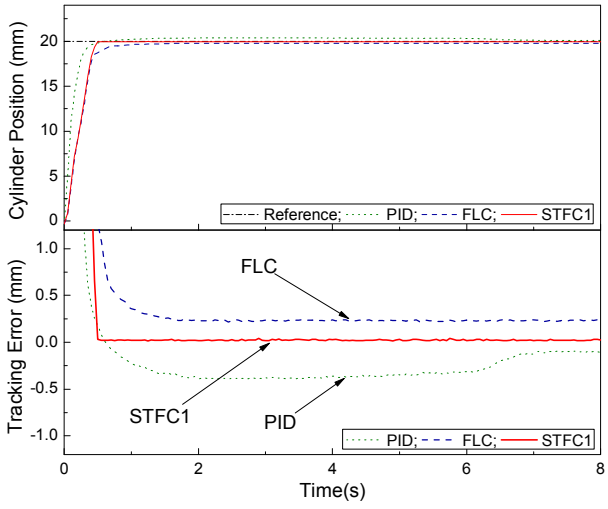

Fig. 14 Comparison of cylinder position responses between using different controllers with respect to a step reference

DOI: XXX-XXX-XXXX

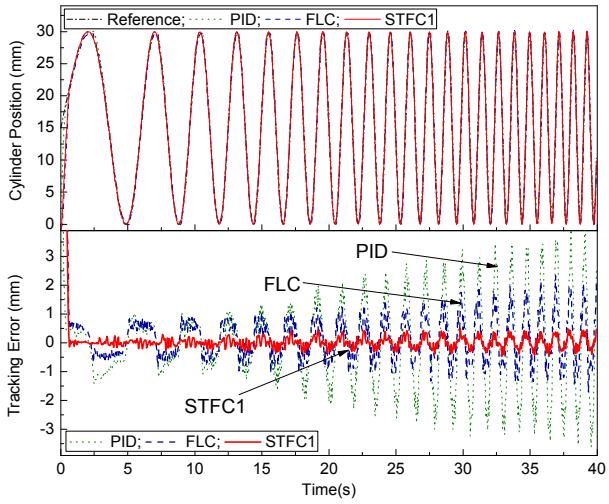

Fig. 15 Comparison of cylinder position responses between using different controllers with respect to a chirp reference

Although the PID could drive the system to the design targets quickly, the performance was not stable due to the system nonlinearities and uncertainties, especially at the higher frequency region in Fig. 15 (see the dot-olive lines). Additionally, the PID gains were tuned for the step reference. Therefore when dealing with the chirp reference, the tracking error increased from 6.67% at 0.1Hz to 23.33% at 1Hz of the working frequency. Comparing with the PID in term of stability, the FLC could bring the better performance (the dash-blue lines). However, the FLC with fixed structure caused the slower response (Fig. 14) and still remained the high control error (13.33% at 1Hz as in Fig. 15). With the designed STFC1, the best tracking results with almost no overshoot, fast rising time and small steady errors were achieved in both cases (the solid-red lines). With the chirp profile, the tracking accuracy using the STFC1 at 0.1Hz and 1Hz was just about ± 0.25mm (1.68%) and ± 0.46mm (3.07%), respectively. This is due to the advanced combination between the fuzzy technique and the proposed SLM.

Second, to clarify the effectiveness of the proposed control scheme, the comparison between the STFC1 and PID controllers were performed with the sinusoidal tracking profiles in which the frequency was regulated as 1Hz, 2Hz, 5Hz and 10Hz while the loading condition was varied using the two springs with stiffness 1kN/m and 8kN/m (see Section 2). By using the same tuning method, the PID gains were tuned for each specific tracking frequency with respect to the 1kN/m load spring to ensure the acceptable tracking performance. The control results were obtained as depicted in Fig. 16. It is clear that in case of the low load condition (1kN/m), the tracking results of both the STFC1 and PID with optimal gains were quite similar. However, when the environment was changed to the higher load (8kN/m), the PID performances were degraded with more undershoots. Meanwhile, the STFC1 with the learning capability could always ensure the stable tracking performances (less than 3.33%). This proves convincingly the applicability of the designed STFC1 to the teleoperation system.

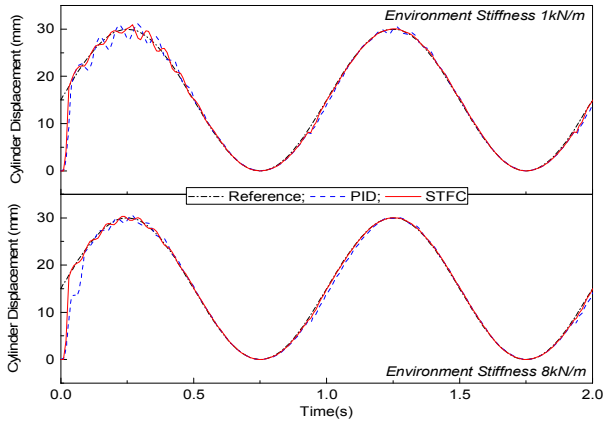

(a) 1 Hz frequency

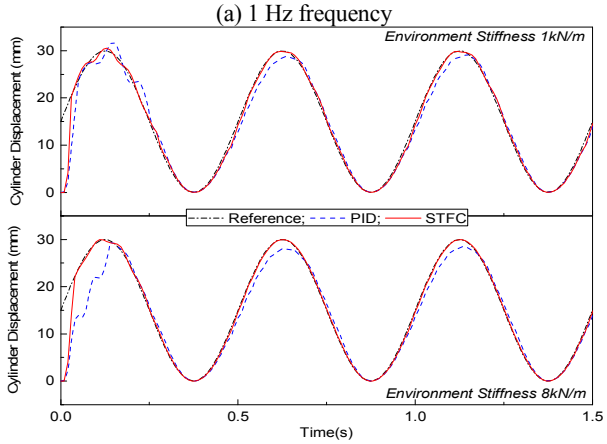

(b) 2 Hz frequency

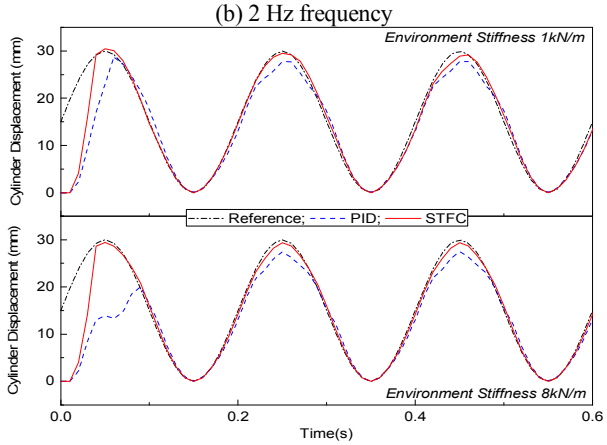

(c) 5 Hz frequency

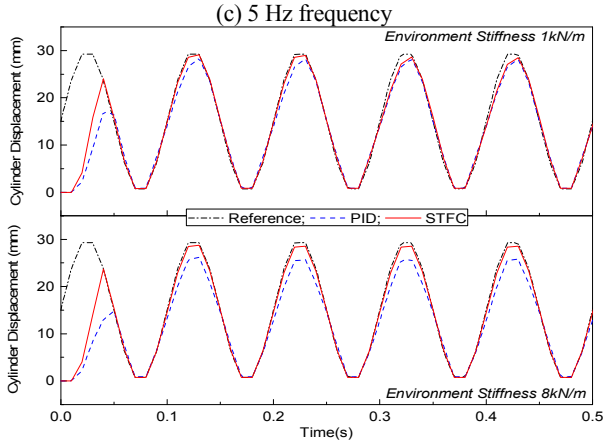

(d) 10 Hz frequency

Fig. 16 Comparison of cylinder position responses between using different controllers with respect to sinusoidal references

4.2 Pressure tracking control

Next, performance of the STFC2 when it was applied to control the reflected pressure of the FRM was inspected by real-time experiments in the similar way as described in the previous section. Two pressure tracking tasks for multi-step and sinusoidal references were chosen in which the sinusoidal with amplitude 2.5bar and frequency 1Hz and 2Hz was selected based on the FRM and joystick dynamics. For these cases, the PID parameters were re-selected properly as $k_p = 3$, $k_i = 1.2$, $k_d = 0.005$ while the STFC2 structure was constructed similarly with that of the STFC1. The input and output scaling factors, g_e, g_{de} and g_u were in turn assigned as 1, 0.007, and 1.2 while the control output offset value u_0 was set to 5.

Subsequently, the experiments with different desired trajectories were performed to obtain the results as presented in figures 17 and 18. The results show the big differences in the tracking performances when using the different controllers. It can be seen that the PID with the fixed gains could not enhance the desired performances when facing with the system nonlinearities and uncertainties. The sudden changes of the desired set-points as well as operation at the higher frequency led to the large overshoots/undershoots (20% to 24%) and large control errors (3% and 20% with respect to the multi-step and 2Hz sinusoidal references) by using this controller.

Comparing to the PID performance, the FLC performance could be improved with the smaller errors (1.2% and 10% with respect to the multi-step and 2Hz sinusoidal references) and smaller undershoots in case of multi-step tracking. However due to the fixed structure use, the FLC could not reduce the overshoots/undershoots over the wide range of working conditions or even, degraded the performance. Both the drawbacks of these controllers could be solved by using the STFC2. Either facing with the multi-step or sinusoidal references, the STFC2 always ensured the most remarkable control results with small overshoots/undershoots and acceptable steady-state errors, 0.8% and less than 4%, respectively. Based on these results, it can be concluded that the designed local controllers are powerful for the teleoperation control application.

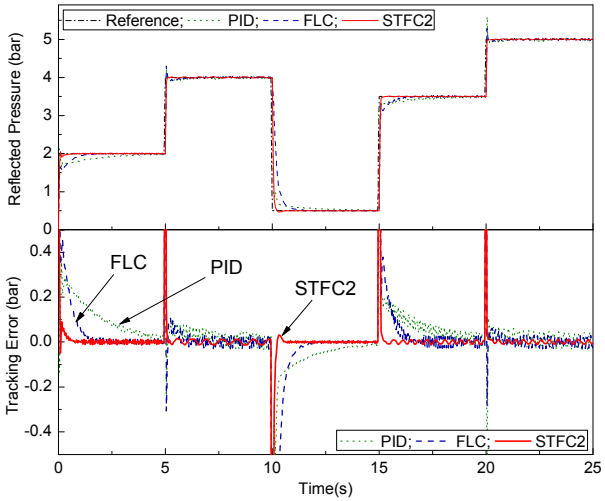

Fig. 17 Comparison of reflected pressure responses between using different controllers with respect to a multi-step reference

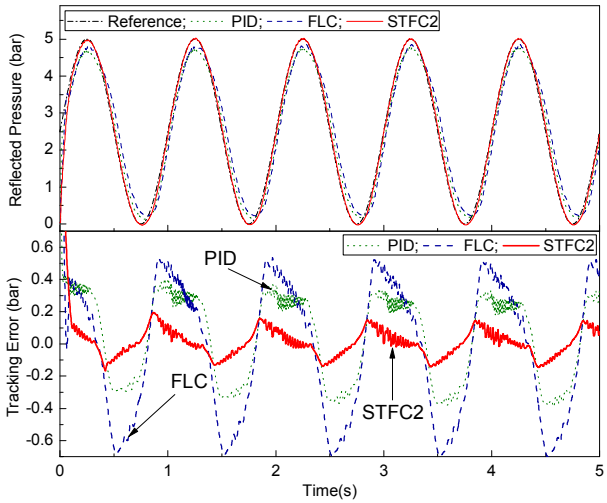

(a) 1 Hz frequency

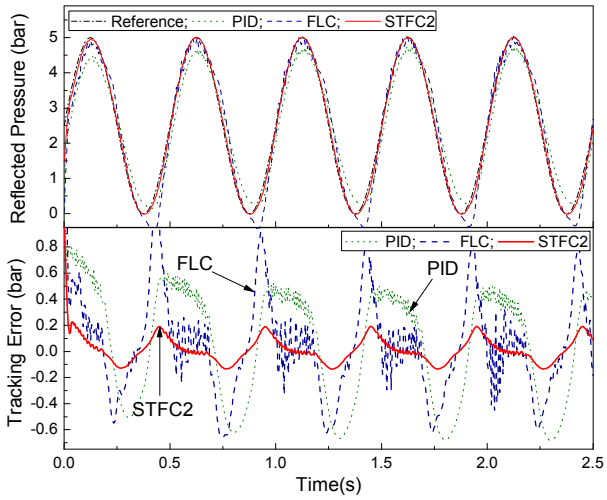

(b) 2 Hz frequency

Fig. 18 Comparison of reflected pressure responses between using different controllers with respect to a 2 Hz sinusoidal reference

4.3 Teleoperation control verification

In order to evaluate the applicability of the proposed FRJC to teleoperation systems, a series of experiments on the testing system was conducted under the different environments. The three different springs (Section 2 with Table 1) and different setting currents for the MR damper were used to simulate environment conditions of six test cases as shown in Table 5. Here, the damping coefficient variation of the MR damper according to the change of the applied current (the forth column of Table 5) was defined based on the previous study on this damper[30]. For each experiment, the joystick commands were randomly given by the operator to drive the slave actuator and, the FRGT was randomly enabled to detect the environment characteristics after the cylinder reached its safety limit (set as 30mm) for the first time. Based on an analysis of the operator's hand dynamics using the trial-and-error method, the transformed factor was properly assigned by 1/100, which means a 100 *N* reflected force was equivalent with a 1 *bar* reflected pressure; and the input and output scaling factors, g_k, g_c and $g_{\tilde{k}_f}$, were assigned as $2.5\text{x}10^{-4}$, $2.5\text{x}10^{-4}$ and 1, respectively.

The experiments were then performed with the six different environments and, the results are plotted in figures 19 from (a) to (f).

DOI: XXX-XXX-XXXX

From these figures, it can be seen that the proposed FRJC behaved well with high accuracy. This comes as no surprise because the FRJC possesses the advanced modules, FRGT and adaptive local controllers, STFC1 and STFC2.

First by using the FRGT, both the damping and stiffness characteristics of each the test condition (Table 5) could be estimated accurately by the RLSM as shown in the first two sub-plots from the top. Based on this information, the FRG was properly generated via the FGT in order to make the similar load feeling to the master site. The tuning performance of the FRG is summarized in the final column of Table 5. This points out that the FRG was automatically regulated according to the environmental characteristics, the smaller value for the harder environment and vice versa. Next, the two local controllers took parts in ensuring the given slave task and FRM task, cylinder position control and reflecting pressure control. The control results, which are in turn depicted in the third and fourth sub-plots, proved remarkably the capability of these controllers. The precisely tracking performances were, therefore, always achieved even dealing with the various loads and disturbances. As a result, the proposed FRJC could ensure the stable performance for the teleoperation system in which the slave executed accurately the desired task while the operator was able to realize truthfully the reacting force or interactions from the environment.

Table 5 Experimental conditions and results of the inferred FRG

Experiment No.	Experiment conditions			FRG (k_f)
	Spring stiffness	MR Damper current	Damping coefficient	
1	1 kN/m	0 A	4kNs/m	1.18
2	1 kN/m	0.2 A	20kNs/m	1.03
3	8 kN/m	0 A	4kNs/m	0.97
4	8 kN/m	0.2 A	20kNs/m	0.63
5	22 kN/m	0 A	4kNs/m	0.65
6	22 kN/m	0.2 A	20kNs/m	0.36

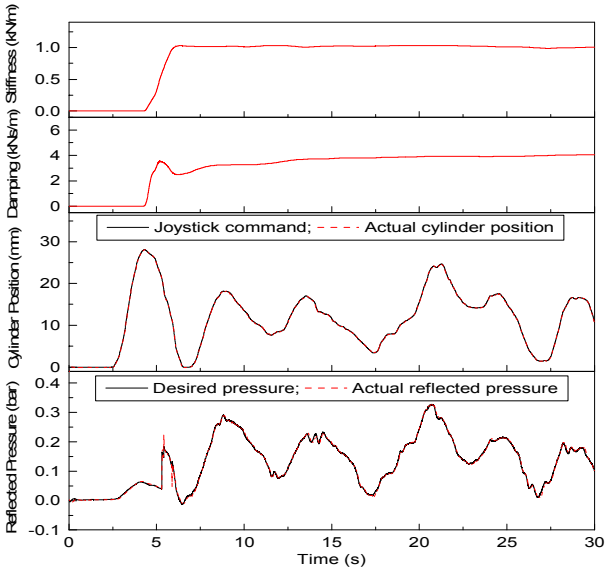

(a) Experiment No. 1

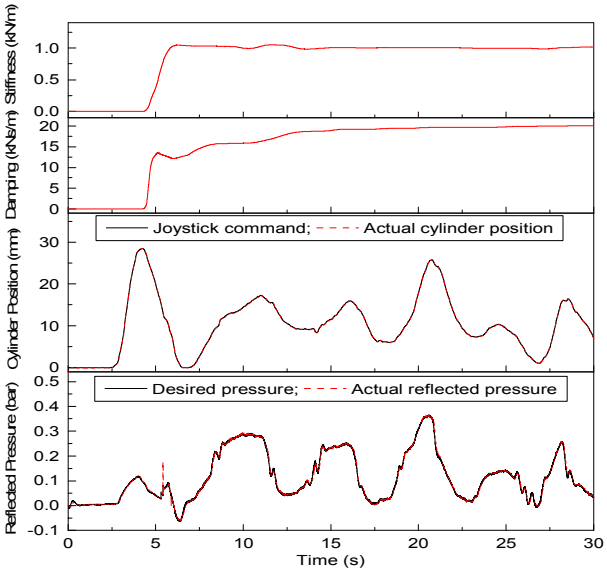

(b) Experiment No. 2

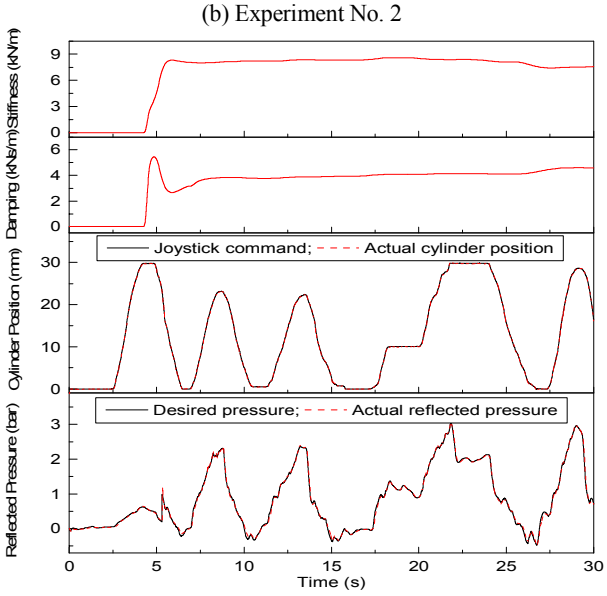

(c) Experiment No. 3

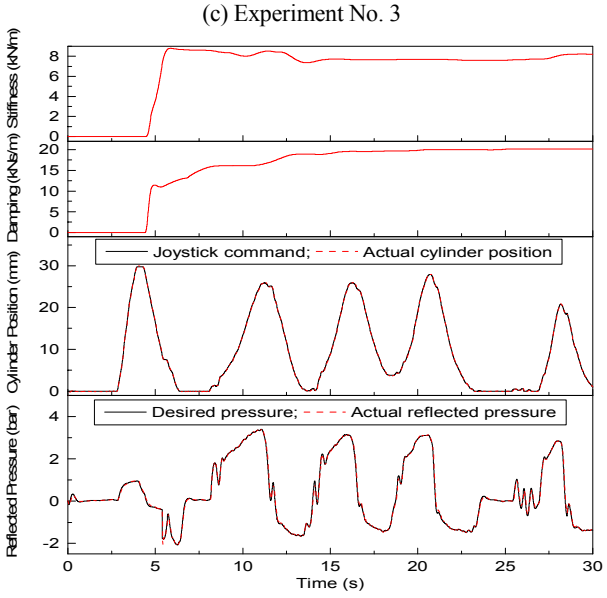

(d) Experiment No. 4

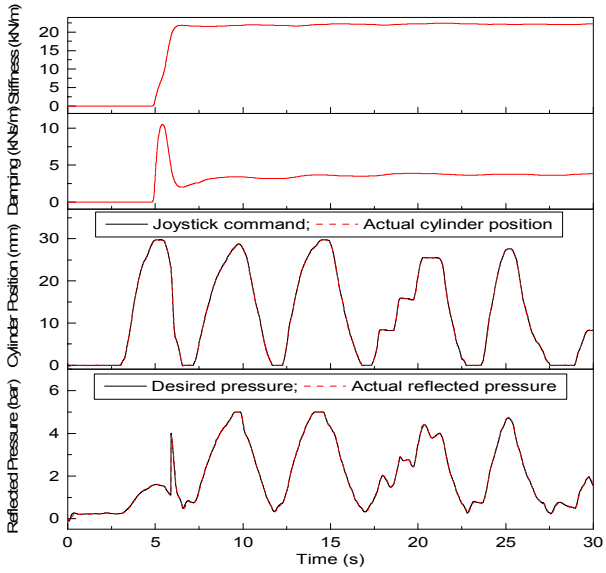

(e) Experiment No. 5

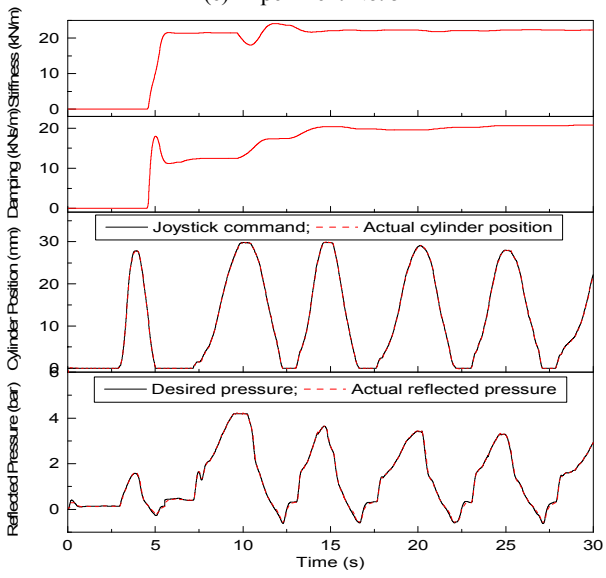

(f) Experiment No. 6

Fig. 19 Teleoperation control performance with different working environments

5. Conclusions

In this paper, the advanced force reflecting joystick control method was presented and successfully developed for applications to bilateral teleoperation systems. The proposed FRJC is the combination of the force reflecting gain tuner and two local adaptive controllers, STFC1 and STFC2. Here, the FRGT is constructed based on the RLSM and FGT to produce properly the FRG which represents the physical interaction between the slave and the environment. Meanwhile, the local controllers are designed and optimized online by the SLM to ensure that the slave follows well given trajectories and to allow the operator to sense truthfully the reflected forces.

The teleoperation test rig was developed to validate the suggested FRJC methodology. Series of real-time control experiments on the test rig were carried out under various environmental conditions to evaluate the effectiveness of the proposed methodology. The results proved convincingly that the FRJC could provide the teleoperation system the good performance with stability. As a future work, development of a FRJC-based teleoperation control system over an imperfect network included delays is carrying out in order to widen its applicability to networked remote applications.

ACKNOWLEDGEMENT

This work is supported by University of Ulsan

REFERENCES

1. Goertz, R.C., “Fundamentals of general purpose remote manipulators,” Nucleonics (U.S.) Ceased publication, Vol. 10, No. 11, pp. 36-45, 1952.
2. Cha, D.H. and Cho, H.S., “A neurofuzzy model-based compliance controller with application to a telerobot system,” Control Engineering Practice, Vol .4, No. 3, pp. 319–330, 1996.
3. Bejczy, A.K. and Kim, W.S., “Predictive displays and shared compliance control for time delayed telemanipulation,” In Proceedings of IEEE International Workshop on Intelligent Robots and Systems, Vol. 1, pp. 407-412, 1990.
4. Kosuge, K., Sata, A. and Furuta, K., “Task-oriented control of master-slave manipulators,” Symposium Flexible Automation, pp. 387-393, 1990.
5. Sarmad, S., Kim, D.S., Choi, Y.S. and Han, C.S., “A novel 3-DOF optical sensor for wearable robotic arm,” International Journal of Precision engineering and manufacturing, Vol. 12, No. 4, pp. 623–628, 2011.
6. Kim, W.S., Hamaford, B. and Bejczy, A.K., “Force-reflection and shared compliance control in operating telemanipulators with time delay,” IEEE Transactions Robotics and Automation,Vol. 8, No.2, pp. 176-185,1992.
7. Venkataraman, S.T., “A neural network based identification of environments models for compliant control of space robots,” IEEE Transactions Robotics and Automation, Vol.9, No. 5, pp. 685-697, 1993.
8. Park, W.I., Kwon, S.C., Lee, H.D. and Kim, J., “Real-time thumb-tip force predictions from noninvasive biosignals and biomechanical models,” International Journal of Precision engineering and manufacturing, Vol. 13, No. 9, pp. 1679–1688, 2012.
9. Jung, K.M., Chu, B.S., Park, S.S. and Hong, D.H., “An implementation of a teleoperation system for robotic beam assembly in construction,” International Journal of Precision engineering and manufacturing, Vol. 14, No. 3, pp. 351–358, 2013.
10. Je, H.W., Baek J.Y. and Lee, M.C., “Current based compliance control method for minimizing an impact force at collision of service robot arm,” International Journal of Precision engineering and manufacturing, Vol. 12, No. 2, pp. 251–258, 2011.
11. Shafiqul, I., Peter X.L. and Abdulmotaleb, E.S., “New stability and tracking criteria for a class of bilateral teleoperation systems,” Information sciences, Vol. 278, pp. 868–882, 2014.

DOI: XXX-XXX-XXXX

12. Hannaford, B. and Wood, L., "Performance evaluation of a 6 axis high fidelity generalized force reflecting teleoperator," In: Proceedings of NASA Conference Space Telerobotics, pp. 87-96, 1989.
13. Gersem, D.G. "Kinaesthetic feedback and enhanced sensitivity in robotic endoscopic telesurgery," PhD Thesis, KU Leuven, 2005.
14. Lawrence, D.A., "Stability and transparency in bilateral teleoperation," IEEE Transactions Robotics and Automation, Vol. 9, No. 5, pp. 624–637, 1993.
15. Lee, J.K., Kim, K.H. and Kang, M.S., "An analysis of static output feedback control for tendon driven master-slave manipulator – Simulation study," International Journal of Precision engineering and manufacturing, Vol. 12, No. 2, pp. 243–250, 2011.
16. Ahn, K.K., "Development of force reflecting joystick for hydraulic excavator," JSME International Journal Series C Mechanical Systems, Machine Elements and Manufacturing, Vol. 47, No.3, pp. 858-863, 2004.
17. Raju, G.J., "Design issues in 2-port network models of bilateral remote manipulation," In: Proceedings of IEEE International Conference Robotics and Automation, Vol. 3, pp. 1316-1321, 1989.
18. Kim, W.S., "Developments of new force reflecting control schemes and an application to a teleoperation training simulator," In: Proceedings of IEEE International Conference Robotic and Automation, Vol. 2, pp. 1412-1419, 1992.
19. Cha, D.H. and Cho, H.S., "Design of a force reflection controller for telerobot systems using neural network and fuzzy logic," Journal of Intelligent and Robotic Systems, Vol. 16, pp. 1-24, 1996.
20. Kuchenbecker, J.K. and Niemeyer, G., "Induced master motion in force-reflecting teleoperation," ASME Journal of Dynamic Systems, Measurement, and Control, Vol. 128, No. 4, pp .800-810, 2006.
21. Polushin, I.G., Liu, P.X. and Lung, C.H., "Projection-based force reflection algorithm for stable bilateral teleoperation over networks," IEEE Transactions Instrumentation and Measurement, Vol. 57, No. 9, pp. 1854 – 1865, 2008.
22. Kim, D.N., Oh, K.W., Lee, C.S. and Hong, D.H., "Novel design of haptic devices for bilateral teleoperated excavators using the wave-variable method," International Journal of Precision engineering and manufacturing, Vol. 14, No. 2, pp. 223–230, 2013.
23. Polushin, I.G., Liu, P.X. and Lung, C.H., "Stability of bilateral teleoperators with generalized projection-based force reflection algorithms," Automatica, Vol. 48, pp. 1005 -1016, 2012.
24. Gong, M., Zhao, D., Feng, S., Wei, H. and Yamada, H., "Force feedback model of electro-hydraulic servo tele-operation robot based on velocity control," In Proceedings of IEEE International Conference Robotic, Automation and Mechatronics, pp. 912-915, 2008.
25. Dimaio, S.P., "A virtual excavator for controller development and evaluation," In: Proceedings of IEEE International Conference Robotics and Automation, Vol. 1, pp. 52-58, 1998.
26. Lee, C.C., "Fuzzy Logic in Control Systems: Fuzzy Logic Controller – Part I," IEEE Transactions Systems, Man, and Cybernetics, Vol. 20, No. 2, pp. 404-418, 1990.
27. Truong, D.Q. and Ahn, K.K., "Force control for hydraulic load simulator using self-tuning grey predictor-fuzzy PID," Mechatronics, Vol. 19, No. 2, pp. 223-246, 2009.
28. Truong, D.Q. and Ahn, K.K., "Self Tuning of Quantitative Feedback Theory for Force Control of an Electro-Hydraulic Test Machine," Control Engineering Practice, Vol. 17, No. 11, pp. 1291-1306, 2009.
29. Yoon, J.I., Truong, D.Q. and Ahn, K.K., "A Generation Step for An Electric Excavator with A Control Strategy and Verifications of Energy Consumption," International Journal of Precision Engineering and Manufacturing, Vol. 14, No. 5, pp. 755-766, 2013.
30. Truong, D.Q. and Ahn, K.K., "Nonlinear black-box models and force-sensorless damping control for damping systems using magneto-rheological fluid dampers," Sensors and Actuators A: Physical, Vol. 167, No. 2, pp. 556-573, 2011.